Radiative Properties of Cirrus Clouds in the Infrared Region

GRAEME L. STEPHENS

CSIRO Division of Atmospheric Physics, Mordialloc, Victoria, Australia 3195.

(Manuscript received 30 May 1979, in final form 4 October 1979)

ABSTRACT

A multiple-scattering radiative transfer model is employed to evaluate the 11 μm and the broad-band infrared (IR) fluxes, cooling rates and emittances in model cirrus clouds for a number of standard vertical atmospheric profiles of temperature and moisture. The single-scattering properties for scattering by mono- and polydispersed randomly orientated long ice columns and for the associated polydispersed equivalent spheres are used in the calculation.

The results reveal IR reflectance at the cloud base of 4% (spheres) and 6% (cylinders). This reflectance modifies significantly the cloud effective emittances, cloud cooling rates and the emission by the total atmospheric column. It is shown that the radiative properties of model cirrus clouds determined under the equivalent sphere approximation represents well the properties determined for scattering by randomly orientated columns. The largest difference between the sphere and cylinder models is for reflectance which is a function of the degree of anisotropy of the scatter. It is shown that the relative contribution to the downward radiative flux at the cloud base (and within the cloud) varied according to the temperature differences between the cloud and the effective radiative temperature of the warmer atmosphere below the cloud. For example, the reflection contribution to the downward effective emittance varies for cylinders (spheres) from 25% (15%) of the total effective emittance in a model tropical atmosphere to 10% (5%) in a subarctic summer model atmosphere.

The existence of IR reflectance from high clouds may account for the previously reported discrepancies between the broad band (effective) emittances derived from observed flux profiles and the theoretical values. The results suggest that the reflectance of high clouds should definitely be included in any parameterization scheme. It appears that the effective emittance is not as useful for high-cloud parameterization as for low-level cloud because of its more pronounced dependence on the temperature structure of the atmosphere.

1. Introduction

Recently, interest has focused on the effects of cirrus clouds on the energy balance of the atmosphere as well as its effects on the remote sensing of atmospheric structure from satellites. Stephens and Webster (1979), for example, showed that the net radiative fluxes at the boundaries of the atmosphere varied substantially for different assumed radiative properties of cirrus clouds used in the radiative transfer calculations. These quantities are important and determine the external forcings of the earth-atmosphere system. Stephens and Wilson (1980) forwarded the hypothesis that the radiative heating associated with high-level clouds is an important forcing function in tropical cloud clusters. Roewe and Liou (1978), in a theoretical study, showed that the presence of a cirrus canopy, even if optically thin, significantly modulates the tropospheric IR cooling rates below the cloud layer. It therefore seems important to understand fully the way in which cirrus clouds modulate both the radiative fields within and surrounding the cloud layer. This paper concentrates only on the modulation of the radiative fields within the cloud layer.

Theoretical and observational investigations of the IR properties of cirrus clouds largely center on the determination of the radiative properties of cirrus clouds in various spectral regions (e.g., Kuhn and Weikmann, 1969; Platt, 1973; Liou, 1974), particularly in the atmospheric window region. Few theoretical studies, apart from that by Roewe and Liou (1978), present broad band radiative transfer calculations.

The broad-band IR properties of cirrus clouds are usually incorporated in dynamic models of the atmosphere or in energy budget studies as a broad band emittance estimated either from observed or theoretically calculated radiative fluxes. It is important to understand how broad band radiative fluxes are modulated in the presence of a cirrus cloud and the sensitivity of this modulation to variations of the assumed cloud structure.

This paper aims to investigate the effect of model cirrus clouds on the IR fluxes and heating rates for the selected wavelength at 11 μm and for broad

0022-4928/80/020435-12$07.00

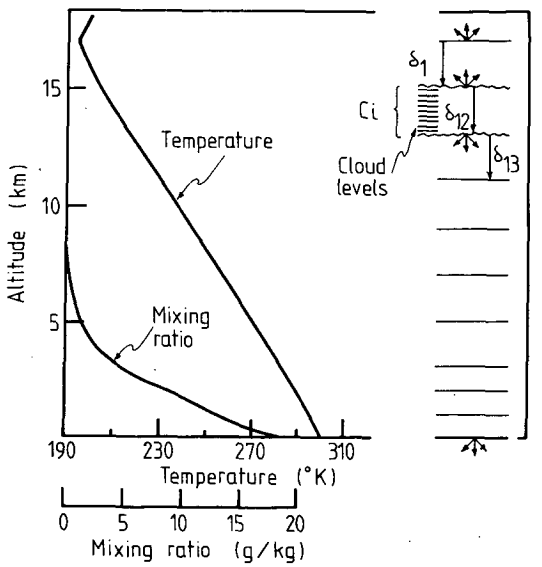

FIG. 1. Vertical profiles of temperature and moisture for the tropical atmosphere. Shown at right are the assumed model levels and cloud positions for the tropical atmosphere.

band calculations. The multiple-scattering calculations are based on the model of Stephens (1978a, model A). The broad band calculations include the 6.3 μm vibration band, rotation band and the 15 μm CO_2 band together with the water vapor partial pressure dependent absorption in the window region. The paper investigates the differences in the derived emittances and cooling rates for a cloud layer composed of either randomly orientated cylinders or spheres of equivalent surface area. The results are presented for a number of standard model atmospheres with particular emphasis on possible ways in which the IR properties of cirrus clouds may be most conveniently parameterized.

2. Model atmospheres

A plane-parallel atmospheric model consisting of 20 levels is employed to evaluate the IR radiative fluxes within the atmosphere. The temperature and water vapor profiles were taken from McClatchey *et al.* (1972) for the tropical, midlatitude summer and winter and the subarctic summer model atmospheres. The vertical profiles of temperature and water vapor are illustrated in Fig. 1 for the tropical model atmosphere.

The cirrus cloud was assumed to be 2 km thick and homogeneous with respect to cloud microphysics. The cloud-top height was assumed to be 2 km below the tropopause of each model atmosphere after the cirrus climatology of Appleman (1961). A schematic view of the model layers is shown to the right of Fig. 1. The 2 km thick cloud layer was divided into 10 layers of equal depth (and optical thickness), while the remaining atmosphere was divided into nine layers and the top of the atmosphere was assumed to be at the tropopause. Each of the model layers were assumed to be isothermal.

The temperature of each layer of the cloud was taken to be the same as that of the environment. The water vapor content of each cloud layer was calculated as the saturated vapor amount over pure ice at the cloud temperature.

The determination of the single-scattering properties of the cirrus cloud layer requires information about the cloud size particle distribution and particle shape. The size distribution measured by Griffith and Cox (1977) for ice crystals in tropical cirrus is employed (reproduced in Fig. 2). They did not sample in the small-particle region. However, small particles, provided that they are sufficiently large in number, may contribute significantly to the extinction of both IR and shortwave radiation. An exponential extrapolation (dashed curve) after Heymsfield (1975) was thus assumed for the small-particle region (Fig. 2).

The ice particles of high cirrus clouds are normally hexagonal columns or bullets and can therefore be usefully approximated by cylinders. The radii of such cylinders were estimated from the crystal length after the relation presented by Heymsfield (1975).

3. Single scattering

The single-scattering phase functions and scattering cross sections were determined using both Mie theory for spheres and the theory for scattering by randomly orientated ice cylinders. As mentioned previously, the predominant shape of ice crystals

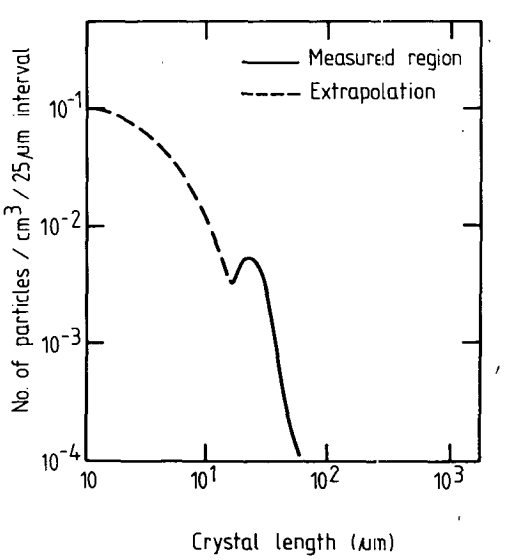

FIG. 2. Particle size distribution for crystals assumed to be 100% columns. The diagram was adapted from Griffith and Cox (1977) illustrating the measured and extrapolated regions.

in cirrus is columnar and the scattering computations were carried out assuming long cylinders with their long axes randomly orientated. The crystal long axes are assumed to be randomly orientated in three dimensions and the resultant single—scattering properties are therefore a three-dimensional average (e.g., Liou 1972b). It is more likely that the crystal long axes are randomly orientated only in the horizontal plane (thus requiring a two-dimensional average). For such cases, the single-scattering properties are functions also of elevation angle. This represents problems in solving the radiative transfer equation and is currently under investigation. However, the scattering calculations for such hypothetical cirrus models, when compared with those deduced from Mie theory, will offer a measure of the sensitivity of the scattering parameters, and ultimately radiative fluxes, to different assumed particle shapes.

The theory of the light-scattering properties of a single long cylinder has been investigated extensively by Liou (1972a,b). Since the theory has been well presented in those papers, only a brief outline is presented below. The scattering and extinction cross sections per unit length for unpolarized light incident on a cylinder at radius r can be defined, respectively, as

$$C_s(\alpha,x) = \frac{2}{k}\left[|b_{01}|^2 + |a_{02}|^2 + 2\sum_{n=1}^{\infty}\left(|b_{n1}|^2 + |b_{n2}|^2 + |a_{n1}|^2 + |a_{n2}|^2\right)\right], \quad (1)$$

$$C_e(\alpha,x) = \frac{2}{k}\mathrm{Re}\left[b_{01} + a_{02} + 2\sum_{n=1}^{\infty}\left(b_{n1} + b_{n2} + a_{n1} + a_{n2}\right)\right], \quad (2)$$

where a_n and b_n are the scattering coefficients (analogous to the Mie scattering coefficients) outlined in some detail by Liou (1972a), x is the size parameter ($x = 2\pi r/\lambda$), r the cylinder radius, k the wavenumber and α the incident angle. The geometry involved in relation to the particle orientation has been outlined by Liou (1972b). The angles responsible for the orientation in the vertical direction ϵ and the horizontal direction γ are related to the incident angle

$$\sin\alpha = \cos\epsilon\cos\gamma. \quad (3)$$

Thus the average scattering and extinction cross sections per unit length for a sample of randomly orientated long cylinders may be expressed as

$$\bar{C}_s(x) = \frac{2}{\pi^2}\int_0^{\pi/2}\int_0^{\pi} C_s(\alpha,x)\,\sec\alpha\,d\epsilon\,d\gamma, \quad (4)$$

$$\bar{C}_e(x) = \frac{2}{\pi^2}\int_0^{\pi/2}\int_0^{\pi} C_e(\alpha,x)\,\sec\alpha\,d\epsilon\,d\gamma. \quad (5)$$

The phase function for a sample of randomly orientated long cylinders when averaged over all orientations with the incident beam unpolarized becomes

$$P(x,\psi_s) = \frac{1}{\bar{C}_s(x)}\int_0^{\pi/2}\int_0^{\pi} i(\psi_s,x,\gamma,\epsilon)\,d\epsilon\,d\gamma, \quad (6)$$

where i is the intensity coefficient for an incident unpolarized light source and ψ_s the associated scattering angle.

The volume scattering and extinction coefficients and phase function, when applied to a volume containing a specific distribution of cylinder sizes, becomes

$$\left.\begin{aligned}\sigma_s &= \int_{x_1}^{x_2} n(x)l(x)\bar{C}_s(x)\,dx\\ \sigma_e &= \int_{x_1}^{x_2} n(x)l(x)\bar{C}_e(x)\,dx\\ \bar{P}(\psi_s) &= \int_{x_1}^{x_2} P(\psi_s,x)l(x)n(x)\,dx\end{aligned}\right\}, \quad (7)$$

where $n(x)$ represents the size distribution of the particles (cylinders or spheres), x_1 and x_2 are the lower and upper limits of the size parameter, respectively, and $l(x)$ is the length of the crystal. Similar expressions can be derived for spheres with the exclusion of $l(x)$ in Eq. (7).

The single-scattering and extinction cross sections and phase functions were determined for randomly orientated cylinders employing the particle size distribution illustrated in Fig. 2 coupled with the radius-length relationships of Heymsfield (1975). The single-scattering properties calculated from Mie theory using spheres of equivalent radii[1] deduced from Fig. 2 were also obtained.

For broad-band calculations, a prohibitive amount of computational effort is required to calculate the scattering parameters in (7) and to integrate over all particle sizes at several chosen wavelengths. Calculations employing the size distribution portrayed in Fig. 2 were performed only for $\lambda = 11$ μm. Broad-band calculations described below were carried out for randomly orientated cylinders of 200 μm length, 30 μm radius and a particle number density of 0.05 cm^{-3} (after Liou, 1974), which roughly represent the crystal parameters expected in high cirrus clouds. The selected wavelengths employed are those tabulated in Stephens (1978a) and the complex refractive indices of ice are taken from Kattawar

[1] The equivalent spherical radius of a particle is $\sim(A/4\pi)^{1/2}$ where A is the surface area of the particle—this equivalent radius is approximately a quarter of the actual crystal length.

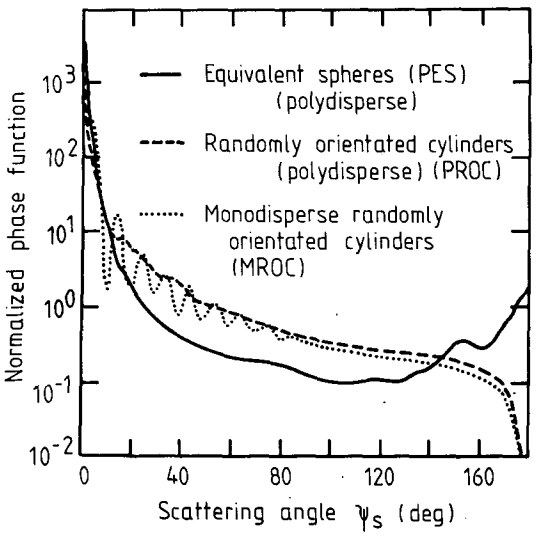

FIG. 3. Normalized phase functions for the assumed particle distributions and types described in the text (PROC, PES, MROC).

and Plass (1968). No concerted attempts are made in this paper to investigate the effects of size distribution on scattered radiation since real particle size distributions are still poorly known for cirrus clouds.

Fig. 3 illustrates the normalized phase functions for polydisperse equivalent spheres (PES) and randomly orientated cylinders and for the given polydisperse size distribution (PROC). The integrations associated with (4)–(6) were performed using a Gaussian 20-point quadrature formula. The necessary convergence criterion adopted were those described by Liou (1972a). For comparison, the normalized phase function is shown for the single cylinder size described above (denoted MROC). The results are presented for $\lambda = 11$ μm and for the complex refractive index of ice from Kattawar and Plass (1968). Specific comparisons between the phase functions of cylinders and spheres have been described in some detail by Liou (1972b). The important differences depicted in Fig. 3 are first that the forward peak for both cylinder cases is significantly suppressed, and second that the glory which is evident for spheres (large spheres) as the scattering angle approaches 180° disappears for cylinders. The essential difference between the two cylinder cases is that the integration over the particle size distribution of the cloud primarily smooths out oscillations evident in the phase function for a single particle.

Table 1 gives the single-scattering properties for the different cloud models at 11 μm. Listed on this table are the volume extinction coefficients (km^{-1}), the single-scattering albedo ($\tilde{\omega}_0 = \sigma_s/\sigma_e$) and the asymmetry parameter ($\langle\cos\psi_s\rangle$). A notable feature is the greater extinction per kilometer for the distribution of cylinders than for either the equivalent spheres or the individual cylindrical crystal extinction. It is also interesting to note that the differences in shape of the phase functions illustrated in Fig. 3 are reflected in the values of the asymmetry parameters. The asymmetry parameter for spheres, as Liou (1974) found, is consistently larger (at all wavelengths) than for scattering by cylinders. This feature is discussed in more detail below. Despite the differences in the case studies portrayed in Fig. 3 and Table 1, the single-scattering albedos are similar.

4. The radiative transfer model

A detailed multiple-scattering radiative transfer model of Stephens (1978a, model A) is employed to calculate the longwave radiative fluxes and radiative heating rates in an atmosphere containing specified cloud layers. Since the model has been discussed extensively elsewhere (Stephens, 1976a, 1978a), only a brief outline is presented here with particular emphasis on changes from the original version of the model.

The model is based on the discrete space theory utilized first in its present form by Grant and Hunt (1968). The specific intensity of radiation is denoted by $I^+(\delta,\mu)$ at an optical depth δ for a beam traveling in a direction which makes an angle whose cosine is δ with the normal in the positive δ direction. $I^-(\delta,-\mu)$ is therefore the intensity of radiation travelling in the reverse direction to that defined by μ.

The discrete representation is established by dividing the optical medium into N layers by $N + 1$ levels (see Fig. 1). Furthermore, we divide $0 < \mu < 1$ into m discrete directions (μ_j). A set of quadrature weights ($C_1, C_2, \ldots, C_m$) is associated with the m discrete directions ($\mu_1, \mu_2, \ldots, \mu_m$). Thus at each level, the column vectors are

$$i_n^+ = \begin{vmatrix} I_{n,1} \\ \cdot \\ \cdot \\ \cdot \\ I_{n,m} \end{vmatrix}, \quad i_n^- = \begin{vmatrix} I_{n,-1} \\ \cdot \\ \cdot \\ \cdot \\ I_{n,-m} \end{vmatrix}, \tag{8}$$

where $I_{n,j} = I(\delta_n,\mu_j)$ and $I_{n,-j} = I(\delta_n, -\mu_j)$. In the

TABLE 1. The derived single-scattering properties for polydispersed randomly orientated cylinders (PROC), equivalent spheres (PES) and a monodispersed randomly orientated cylinder of radius 30 μm, length 200 μm, and assumed particle density of 0.05 cm^{-3} (MROC). The refractive index for ice was assumed as 1.29-i0.0954.

	σ_e (km^{-1})	$\tilde{\omega}_0$	$\langle\cos\psi_s\rangle$
Cylinders (PROC)	1.99	0.525	0.728
Spheres (PES)	1.66	0.512	0.872
Cylinders (MROC)	1.23	0.517	0.787

context of radiation flowing through an atmospheric layer, the positive sign refers to the *downward* directed radiances and the negative sign to *upward* radiances.

The complete internal radiance field may be determined in an efficient manner by the simple recursive algorithm (Grant and Hunt, 1968)

$$i^+_{n+1} = R(1, n+1)i^-_{n+1} + V^+_{n+1/2}, \quad (9)$$

$$i^-_n = T(n, n+1)i^-_{n+1} + V^-_{n+1/2}, \quad (10)$$

where

$$T_{n+1/2} = [I - R(n+1, n)R(1,n)]^{-1},$$

$$R_{n+1/2} = T(n+1, n)R(1,n)T_{n+1/2},$$

$$R(1, n+1) = R(n, n+1) + R_{n+1/2}T(n, n+1),$$

$$\hat{T}(n, n+1) = T_{n+1/2}T(n, n+1),$$

$$T'_{n+1/2} = [I - R(1,n)R(n+1, n)]^{-1},$$

$$\hat{T}(n+1, n) = T(n+1, n)T'_{n+1/2},$$

$$\hat{R}(n+1, n) = R(n+1, n)T'_{n+1/2}, \quad (11)$$

and

$$V^+_{n+1/2} = \hat{T}(n+1, n)V^+_{n-1/2} + J^+_{n+1/2} + R_{n+1/2}J_{n+1/2},$$

$$V^-_{n+1/2} = \hat{R}(n+1, n)V^+_{n-1/2} + T_{n+1/2}J_{n+1/2},$$

for $n = 1, 2, \ldots N$, with the initial conditions

$$R(1,1) = 0 \quad \text{and} \quad V^+_{1/2} = i^+_1.$$

In these equations $R(n, n+1)$, $T(n, n+1)$ and $J^{\pm}_{n+1/2}$ are the diffuse reflection, transmission and source function operators for the layer bounded by levels n and $n+1$. Eqs. (9) and (10) can therefore be directly related to the radiative transfer equation for thermal radiation through the principles of invariance. The various operators have been discussed at length by others (e.g., Wiscombe, 1976) and are generated from the single-scattering phase functions and scattering and extinction cross sections by employing doubling techniques. The single-scattering data employed in the model were discussed in the previous section and the phase function, normalized to unity, was incorporated into the operators using the delta M method of Wiscombe (1977).

The radiances determined from (10) and (11) are used to provide the radiant fluxes

$$H^{\pm}(\delta_n) = 2\pi \sum_{i=1}^{m} C_i \mu_i I_{n,\pm i}. \quad (12)$$

Broad-band fluxes are then obtained by an integration of the fluxes obtained by Eq. (12) across the IR spectrum or the portion of the spectrum of interest. The spectrum between 4 and 100 μm was divided into 20 intervals, nine for the vibration band, four for the atmospheric window and seven across the water vapor rotation band. The CO_2 band was overlapped with the rotation band interval centered at 15 μm. The subdivision of the vibration and rotation bands follows Rodgers and Walshaw (1966). Molecular absorption was included in the multiple-scattering model using the exponential sum techniques summarized in more detail by Wiscombe and Evans (1977). The molecular absorption in each model layer of the atmosphere is simulated by a series of M pseudo-monochromatic solutions. The computational aspects are therefore the same as model A of Stephens (1978a) and is very similar to that of Roewe and Liou (1978).

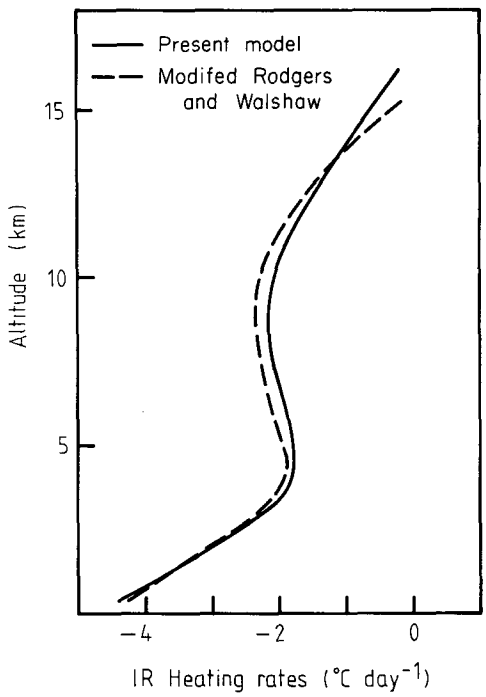

FIG. 4. Comparison of the calculated clear sky cooling rates by the two models described in the text.

Fig. 4 shows a comparison between the clear sky broad band cooling rates calculated by the present model to those of the modeled Rodgers and Walshaw model (Stephens, 1976b). Only 10 atmospheric layers were used for the vertical resolution of the present model (compared to 24 used in the Rodgers and Walshaw type calculation). The vertical structure within the region of the cloud layer (Fig. 1) was removed and only one clear sky layer was assumed for this region. Data for the computations are from the tropical atmosphere shown in Fig. 1. Agreement is particularly good considering the broader vertical resolution adopted in the present model. The results shown in Fig. 1 are similar to those of Roewe and Liou (1978) and it is reasonable to expect that the broad-band incident fluxes at the cloud boundary are well handled by the model. However, as emphasized in Roewe and Liou,

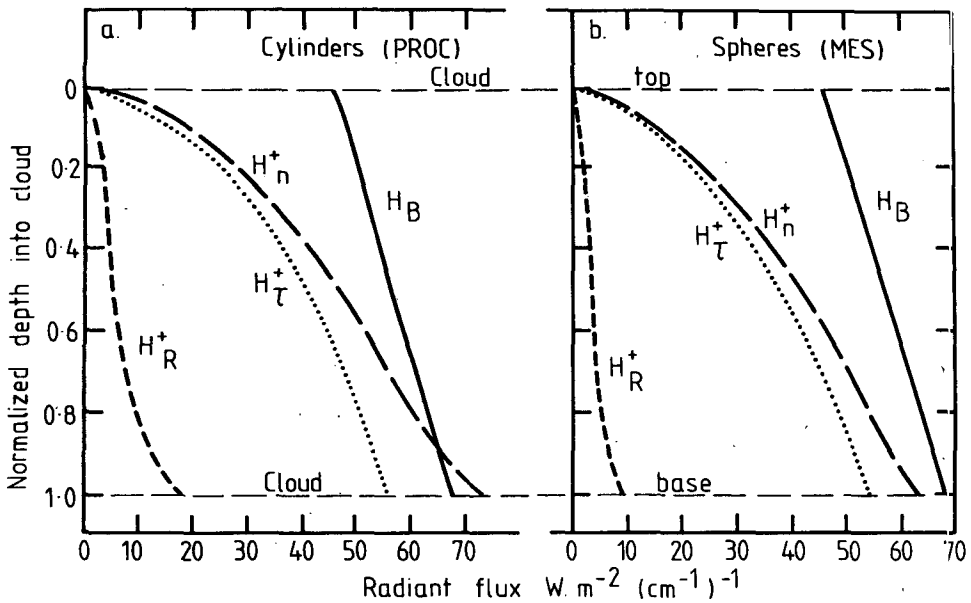

FIG. 5. Radiative flux profiles and the reflection and emission components in a model cirrus cloud in a tropical atmosphere for PROC (a) and PES (b). Included for reference is the cloud blackbody flux profile.

problems are likely to arise when the model is employed to calculate the clear sky cooling rates for small optical paths. This is not likely to be a concern in this study since the clear-sky calculations are employed only to provide the requisite cloud boundary incident fluxes and the radiative fields are analyzed only within the cloud layer.

5. Results

Calculations were carried out of the transfer of IR radiation through an atmospheric column possessing a specified cirrus cloud layer for 16 discrete emergent angles. It is probable that the radiative properties of high clouds (as for lower level water clouds) are largely determined by the atmospheric window region. The remote sensing of surface temperature also utilizes the radiative properties in the window region. Thus calculations were first carried out at 11 μm. These calculations assume the size distribution presented in Fig. 2 for cylinders and adapted for equivalent spheres. The variation of the radiative properties across the window are comparatively small (Liou, 1974) and the calculations at 11 μm are therefore taken to be representative of the atmospheric window. To obtain the broad-band IR properties of model cirrus clouds the calculations were then extended across the IR spectrum. The broad-band calculations were performed assuming the equivalent sphere approximation for polydispersed cloud particles (PES) described in Fig. 2 and also for a monodispersed randomly orientated cylindrical ice crystal (MROC).

a. The 11 μm flux profiles in model cirrus clouds

The results presented below concentrate primarily on the downward fluxes within the cloud layer and, in particular, at the cloud base. The latter quantity is an important parameter in radiation balance studies especially at the earth's surface. The downward flux profiles in a model cirrus cloud layer 2 km thick for the tropical atmosphere of McClatchey *et al.* (1972) are shown in Figs. 5a and 5b for the case of scattering by cylinders and spheres, respectively. The contributions to the downcoming radiance by reflection of the incident upwelling radiance [i.e., $R(1, n+1)i_{n+1}^-$ in Eq. (10)] and the combined transmitted and emitted component (i.e., $V_{n+1/2}^+$) are included on the diagram in flux form together with the blackbody flux and the total flux. The various fluxes shown on the diagrams are formally defined for any layer as

$$\left.\begin{aligned} H_\tau^+ &= 2\pi \sum_{i=1}^{m} C_i \mu_i (V_{n+1/2}^+) \\ H_R^+ &= 2\pi \sum_{i=1}^{m} C_i \mu_i [R(1, n+1) i_{n+1}^-] \\ H_B &= \pi B_\lambda(T) \\ H_n^+ &= H_\tau^+ + H_R^+ \end{aligned}\right\}, \quad (13)$$

where H_τ represents the flux component due to the combined cloud transmission and emission. Since at $\lambda = 11$ μm the downward irradiance at the cloud top is negligible, H_τ thus represents the flux com-

ponent due to emission only. H_R is the contribution to the downward directed flux by reflection of the upward irradiance. A striking feature of Figs. 4a and 4b is that the contribution to the total flux H_n^+ by reflection of the upward irradiance is a significant fraction of H_n^+ particularly for scattering by cylinders. As a result, the total flux density for $\lambda = 11$ μm at cloud base for the cylinders case exceeds the blackbody flux.

Table 2 is presented to compare the flux emittances and reflectances at 11 μm for the two cases portrayed in Fig. 5. The flux emittance and reflectance were respectively determined from

$$\left.\begin{aligned} \epsilon_F &= H_\tau/\pi B_\lambda(\bar{T}) \\ \rho_F &= H_R/E^- \end{aligned}\right\}, \qquad (14)$$

where H_R and H_τ are the flux components described by Eq. (13) at the cloud base, E^- is the *irradiance* at cloud base (i.e., the incident upward flux at cloud base) and $\bar{T}$ the temperature of the cloud taken as the mean temperature along the vertical path above cloud base. Also included in Table 2 are the ratios of the upward and downward *exitances* M (i.e., the total flux composed of transmitted, reflected and emitted components) at cloud top and base, respectively, to the irradiance at cloud base (E^-).

The reflectance at cloud base as defined by Eq. (14) is only 3% for scattering by spheres and 5% for cylinders. The differences between the case studies involving spheres and cylinders for the quantities shown in Table 2 are generally small. It is acknowledged here that the small differences in optical depths between the sphere and cylinder case studies implies that a strict comparison between the two should result in small differences in the calculated radiative properties of the clouds. Cases were run for which the volume extinctions of the PROC case were used with the scattering functions derived for the spheres. These results are also listed on Table 2 in parentheses. The changes to the quantities so computed are small and the contrasts in the reflectances, as portrayed in Figs. 5a and 5b and in the following diagrams are not accounted for by the small differences in optical depth. Although the quoted reflectances are small, Figs. 5a and 5b indicate that the contribution to the total flux in the cloud by reflectance is large (25% of the total flux at cloud base for cylinders and 15% for spheres). This contribution is particularly marked for high clouds because the cloud base irradiances (E^-) are larger than the blackbody fluxes within the cloud.

The ratios of $M^\pm/E^-$ shown in the table provide the ratios of the fluxes leaving the cloud boundaries to the incident (upward) irradiance at cloud base. In particular, M^-/E^- must not be misconstrued as a cloud transmittance but is a combination of transmittance, emittance and reflectance processes. Since $E^- - M^+$ is the net flux (upward) at the cloud base and M^- is the net flux at cloud top (assuming no downward incident flux at the cloud top), the comparison of M^+/E^- and M^-/E^- will indicate the amount of energy lost or gained by the cloud layer. The values shown in Table 2 suggest that the cloud layer gains IR radiative energy (~60% of the upward irradiance E^-). Thus net energy gain for high cloud in the tropics contrasts the net energy loss of lower level clouds (e.g., Stephens, 1978a).

TABLE 2. Comparison (%) of the 11 μm emittance, reflectance and the upward and downward exitances (M) expressed as fractions of the upward irradiance at cloud base (E^-). The calculations were performed for a 2 km thick polydisperse model cirrus cloud in a tropical atmosphere.

Radiative property	Spheres (PES)	Cylinders (PROC)
Emittance ϵ	95 (98)	98
Reflectance ρ_F (11 μm)	3 (3)	5
(M^-/E^-)	22 (19)	18
(M^+/E^-)	19 (20)	22

b. The 11 μm effective emittance

A useful concept that has emerged over the past few years is that of effective emittance which defines a form of emissivity determined from the layer exitance. The definition of effective emittance inseparably combines the effects of reflection, emission and transmission and therefore includes the effects of the upward flux (i.e., surface temperature) below the cloud. The concept and its potential usefulness have been discussed previously (e.g., Stephens, 1978b).

The impact on emittance of the scattering properties described in Section 3, with particular emphasis on the reflectance component, can be assessed from Figs. 6a, 6b and Fig. 7. Figs. 6a and 6b portray the downward effective emittance as a function of normalized optical depth for scattering by cylinders and spheres respectively. The effective emittance in this case is defined (for negligible downward flux at the cloud top) as

$$\epsilon_e^+ = \frac{H_{(n)}^+}{\pi B(\bar{T})}, \qquad (16)$$

where n in this context refers to the level of interest in the cloud layer. The effective flux emittances

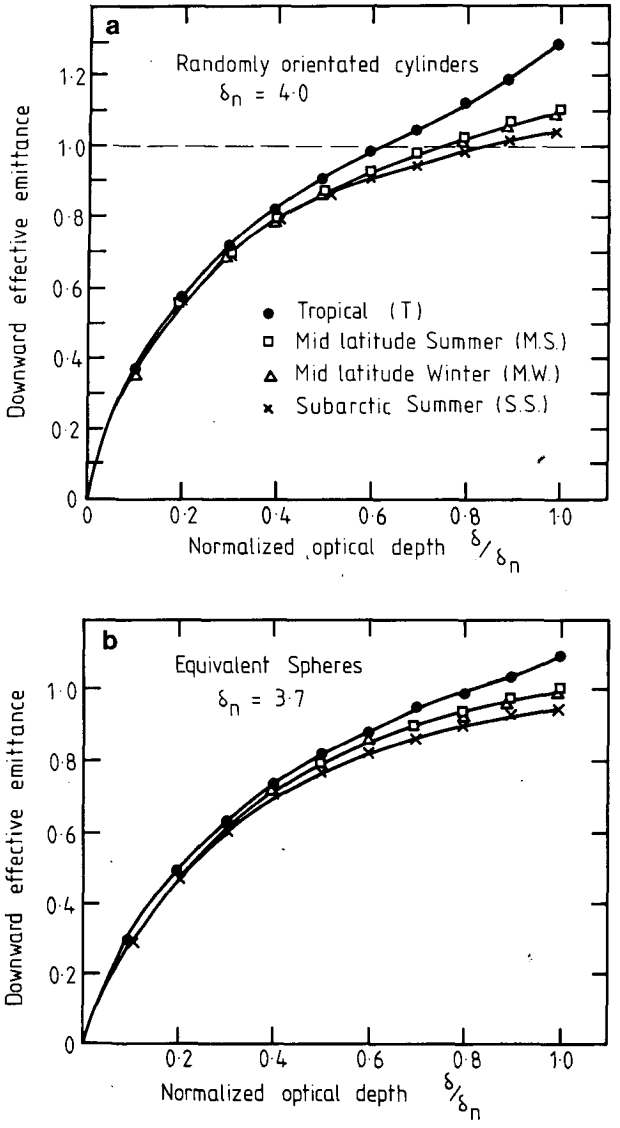

FIG. 6. Downward effective emittance as a function of normalized optical depth for a model cirrus cloud PROC cylinders (a) and PES spheres (b). Calculations were carried out for the four model atmospheres listed.

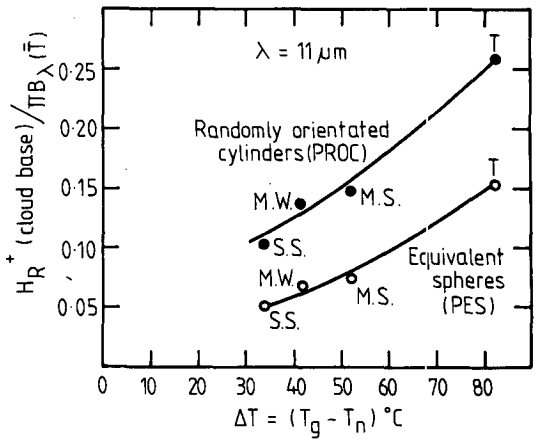

FIG. 7. The contribution to the downward effective emittance for λ = 11 μm by the reflection of the cloud base irradiance as a function of the temperature difference between cloud base (T_n) and the lower underlying surface (T_g).

displayed in Fig. 6 were determined for a 2 km thick layer cloud assuming the four model atmospheres listed on the diagrams. The effective emittance for the case of scattering by cylinders exceeds unity at the cloud base for all model atmospheres with the largest departure occurring for the tropical atmosphere. On the other hand, the effective emittance for spheres exceeds unity only for the tropical atmosphere. The concept of an effective emittance >1 is not new. For example, Feigelson (1970) has noted that the downward IR radiation from dense cirrostratus can exceed blackbody radiation.

The reason for an effective emittance larger than 1 is that the upward irradiance which is reflected by the cloud originates largely from the earth's surface. The reflected component of the total flux is a significant fraction particularly for scattering by cylinders despite the relatively small reflectance ($\rho_F \approx 5\%$). An estimate of the contribution by reflection to the effective emittance can be obtained by comparing the emittance listed in Table 2 to the effective emittance at cloud base shown in Figs. 6a and 6b. This contribution will decrease as the effective radiative temperature of the underlying atmosphere and surface decreases.

Fig. 7 portrays the contribution to the downward effective emittance by reflection at the cloud base [i.e., the ratio $H_R^+(n)/\pi B(\bar{T})$] as a function of the temperature difference between the surface and cloud base for the four model atmospheres. This diagram confirms that the smaller the effective temperature of the underlying atmosphere and surface, the smaller is the reflected contribution to the total downward flux. It is important to note that the reflection by cylinders (and spheres for that matter) contributes a significant percentage of the total effective emittance within the range of $T_g - T_n$ typical for cirrus clouds.

c. The effect of phase function anisotropy on ρ_F

The IR reflectance properties of cirrus clouds, although small for the case studies described above, have a significant impact on cloud effective emittances and thus on the amount of radiative energy directed toward the surface or emitted to space. These quantities are important for radiation budget studies. It therefore seems important to determine the sensitivity of ρ_F to the basic scattering properties described by the scattering phase function. Such a sensitivity study is particularly valid in this context since the scattering phase functions

for real crystal clouds are still relatively poorly known.

The sensitivity of ρ_F to the assumed phase function was performed by employing a Henyey Greenstein function of the form

$$\gamma_s(\cos\psi_s) = \frac{1 - g^2}{1 + g^2 + 2g\cos\psi_s}, \qquad (17)$$

in which $g = \langle\cos\psi_s\rangle$ can vary from -1 (complete backscatter) through $g = 0$ (isotropic scattering) to $g = +1$ (fully forward scattering). Ice crystal clouds are likely to possess an asymmetry parameter in the range $0 < g < 1$. Phase functions were determined by Eq. (17) for a number of values of g in this range and were applied to the radiative transfer model assuming the same conditions relevant to Fig. 5 for the values of $\tilde{\omega}_0$ and δ_n specified for equivalent spheres in Table 1.

The calculated reflectance ρ_F is shown in Fig. 8 as a function of $1 - g$. The reflection by anisotropic scatter can be considered as a function of the scaled optical depth $(1 - g)\delta$ (Van de Hulst and Grossman, 1968). Thus the reflectance for a given δ then reduces to a function of $1 - g$ which is a useful way of comparing results obtained with different phase functions. Fig. 8 indicates that the reflected flux at cloud base is directly related to the degree of anisotropy of the scattering phase function. The asymmetry parameters derived for scattering by cylinders (both in the IR and visible) are consistently smaller than those determined from Mie theory [i.e., see Table 1 and Liou (1974)]. Thus a cloud whose particles are approximated by cylinders will reflect more than for spherical cloud particles. It is possible that the asymmetry parameter for ice crystal clouds in the real atmosphere could be even smaller than those presented in Table 1. For example, a phase function with $g = 0.5$ leads to a reflectance of $\rho_F \approx 9\%$, which will accordingly enhance the cloud-base exitance.

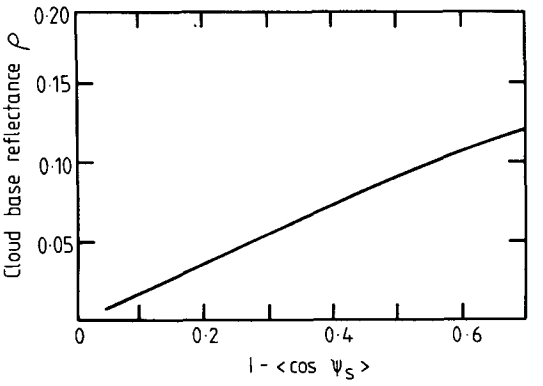

FIG. 8. The cloud base reflectance ρ_F for $\lambda = 11$ μm as a function of $1 - \langle\cos\psi_s\rangle$.

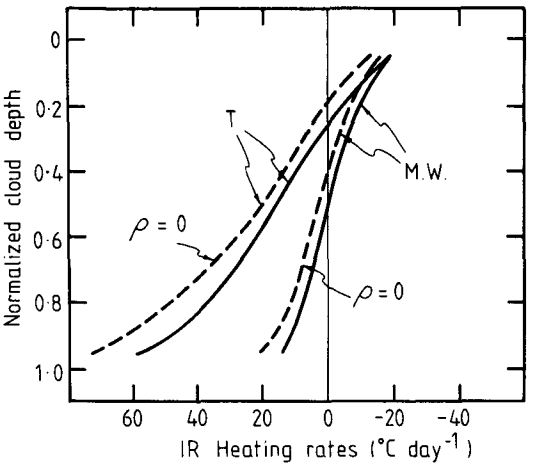

FIG. 9. Broad-band IR heating rates in a model cirrus cloud for MROC for the two model atmospheres listed. Comparison is shown for heating rates determined with and without cloud reflectances.

d. Broad-band calculations

Fig. 9 shows comparisons of the longwave cooling and heating profiles in the model cirrus cloud for the tropical (T) and midlatitude winter (MW) model atmospheres. The profiles depicted on Fig. 9 use the single cylinder size and concentration shown in Table 1 (MROC). The solid line applies to calculations which include reflection and the dashed curves apply for calculations in which reflection was set to zero.

Fig. 9 indicates that the IR heating rates, particularly at the cloud base, are significantly different when reflection is included. The tendency is for an enhanced IR heating in the lower portions of the cloud for the case of no reflection. This results from the larger net irradiance at cloud base originating from the atmosphere below. Accordingly, the heating rate differences are larger for the tropical case study.

The broad-band emittances, reflectances and the ratios of the broad-band upward and downward exitances at cloud top and base to the cloud base broad-band irradiances are presented in Table 3. The results shown on the table correspond to the broad-band flux calculations for model cirrus clouds for the PES and MROC case studies and for the model atmospheres described above. (Note that the

TABLE 3. As in Table 2 but for the broad-band fluxes. The calculations were performed for PES and MROC (in parentheses)

Atmosphere model	ϵ	ρ	M^+/E^-	M^-/E^-
Tropical	92(90)	4(6)	35(34)	34(39)
Midlatitude summer	92(90)	4(6)	58(53)	52(55)
Midlatitude winter	92(90)	4(6)	57(54)	54(57)
Subarctic summer	92(90)	4(6)	67(65)	68(69)

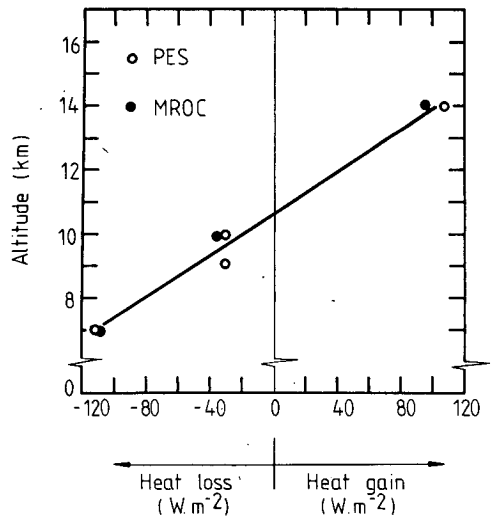

FIG. 10. Net radiative gain (W m^{-2}) for a model cirrus cloud at various heights in the model atmospheres displayed. Calculations were carried out for MROC and PES.

cylinder case study in Table 2 is for PROC and not MROC.)

The broad-band emittances and reflectances are only slightly different from the 11 μm values in Table 2 due to the variations of volume extinction coefficients and asymmetry parameter across the IR spectrum. The ratios of the broad-band exitances to upward irradiance for the tropical case study are significantly different than for the respective 11 μm values. This difference may be attributed to the effects of the intervening atmosphere between the cloud and the surface. The relative net input of energy into the cloud base from the broad-band flux is smaller than for the 11 μm flux since the former effectively originates from a level (and temperature) more adjacent to the cloud level (and temperature). This feature accounts for the differences in net energy gained by the cloud ranging from 60% of the 11 μm cloud-base irradiance to 30% of the broad-band irradiance at cloud base.

Fig. 10 shows the net energy gained by the model cloud layer as a function of altitude (taken as the mean of the cloud top and cloud base altitudes) for the PES and MROC case studies. The lower cirrus layer in the subarctic summer atmosphere is radiatively cooled because the upward flux from the cloud top exceeds the net input to its base. The situation is reversed for the higher cirrus layer in the tropical atmosphere which displays a net radiative energy gain.

Stephens and Webster (1979) indicated that the presence of cirrus clouds significantly affects the radiative fluxes at the boundaries of the atmosphere. These quantities are important in climate studies since they are an indication of the direct external forcing of the earth-atmosphere system. Table 4 presents the longwave fluxes (4–100 μm) at the earth's surface and at the top of the atmosphere (taken as the tropopause) for the four model atmospheres listed. The results in the table correspond to broad-band flux calculations for model cirrus clouds for the PES and MROC case studies. Also included in the table in parentheses are the fluxes determined assuming zero IR reflection by the cloud layer. Listed on the table is net IR flux at the surface, net flux at the top of the atmosphere and the difference in net flux at the two boundaries, all values in W m^{-2}. The latter entry is therefore an important quantity representing the total longwave emission from the atmosphere.

Comparison between two cases shows larger net fluxes at the surface and a smaller net flux at the top of the atmosphere when $\rho = 0$. The changes in the net flux at the surface in the tropics are only marginal since the larger amounts of water vapor effectively shield the surface from the cloud layer in the upper troposphere. Note that the assumption of no reflection when compared to the relatively small broad band reflectances of spheres (4%) and cylinders (6%) effect the net IR fluxes in the opposite sense at the two boundaries of the atmosphere. Thus the net flux difference, being a smaller residual of two relatively large quantities, is significantly altered.

The differences in ΔH for the reflection (no reflection) comparison are large for the tropical atmosphere varying from $-41(-27)$ W m^{-2} for model spheres to $-58(-42)$ W m^{-2} for model cylinders. The differences in ΔH from spheres to cylinders largely result from different extinction coefficients as evident in Table 1.

e. Broad-band emittances

The downward and upward broad-band emittances are shown respectively in Figs. 11a and 11b as a function of ice water path (IWP). These emittance profiles were derived for the input data relevant to the results for the tropical atmosphere model presented in Table 4 assuming a cirrus cloud of monodispersed randomly orientated cylinders (MROC). The dashed curves on each diagram represent the emittances derived from the formal definition of Eq. (15) and therefore includes only the emitted flux contributions. The solid curves, on the other hand, represent the effective emittance which combines emission and reflection. Thus a comparison between the two curves shown in each diagram is indicative of the effect of IR reflectance on the assumed emittance. The differences are significant for both downward and upward directed radiation.

The shaded region in Fig. 11a represents the relationship of Griffith and Cox (1977) for downward emittance deduced from flux measurements in tropical cirrus cloud. The extent of the shaded envelope represents the 90% confidence limits for their observations. The emittances deduced by Griffith

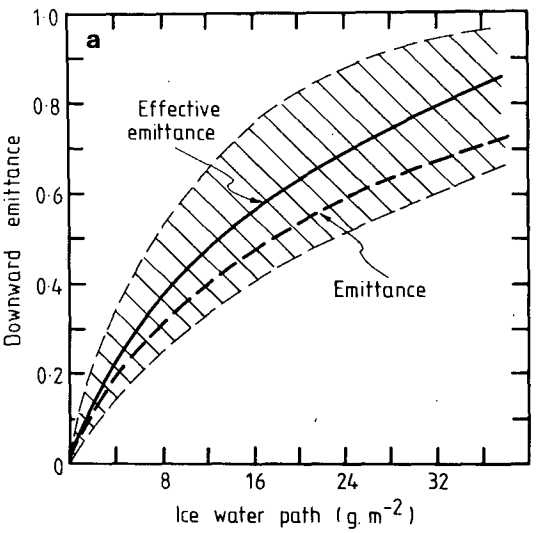

FIG. 11a. Downward emittance as a function of the ice water path determined for MROC. Shown on the diagram are the relationships derived for effective emittance (solid line) and emittance (dashed line). The shaded envelope corresponds to the 90% confidence limits for the relationship derived by Griffith and Cox for (effective) emittance determined from observation.

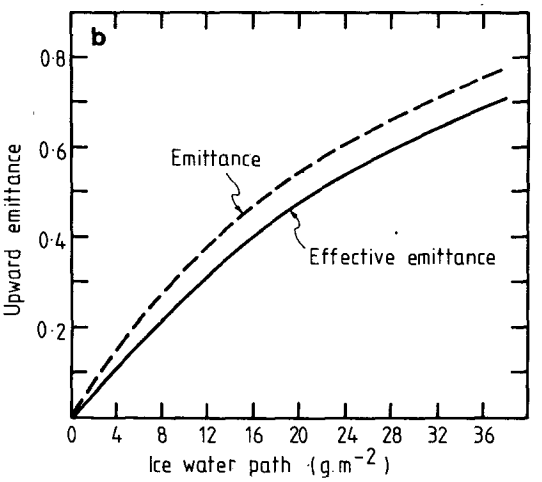

FIG. 11b. As in Fig. 11a except for upward emittance.

and Cox from the measured flux profiles are essentially effective emittances which include contributions from IR reflectance. It appears that the discrepancies reported by Griffith and Cox between their emissivities and the theoretical values, evident by comparing the position of the dashed curve in relation to the envelope, may be partially attributed to IR reflectance. However, reflectance cannot explain fully the discrepancies reported by Griffith and Cox. Their observations were made in essentially undercast sky conditions and the underlying radiative temperature background in this case would be smaller than for clear sky conditions below the cloud layer, reducing the contribution by reflectance.

6. Conclusions

A multiple-scattering radiative transfer model has been employed to evaluate both the 11 μm and broad-band IR fluxes, cooling rates and emittances in model cirrus clouds for a number of standard vertical atmospheric profiles of temperature use and moisture. The single-scattering properties were evaluated for scattering by mono- and polydispersed, randomly orientated, long-column ice crystals and for the associated polydispersed equivalent spheres.

The results reveal IR broad-band reflectances at

TABLE 4. Comparison of the broad-band longwave fluxes at the top (H_0) and bottom ($H_g^{\pm}$) of the atmosphere possessing a 2 km thick cirrus layer with a cloud top 2 km below the tropopause for the four model atmospheres listed. Also presented are net fluxes at the atmospheric boundaries (positive downward) and net flux differences (ΔH). Calculations are presented for the PES and MROC case studies (see Table 1). All quantities are in W m^{-2} and comparison is made for the case when cloud IR reflectance set to $\rho = 0$ (in parentheses).

Equivalent spheres $\rho_F = 4\%$					Randomly orientated cylinders $\rho_F = 6\%$				
H_g^+	H_g^-	$H_g^+ - H_g^-$	H_0^-	ΔH	H_g^+	H_g^-	$H_g^+ - H_g^-$	H_0^-	ΔH
				Tropical					
388	−465	−77	−118	−41	388	(−465)	−77	−135	−58
(384)	(−465)	(−81)	(−108)	(−27)	(383)	(−465)	(−82)	(−124)	(−42)
				Midlatitude summer					
351	−430	−79	−172	−93	349	−430	−81	−181	−100
(346)	(−430)	(−84)	(−162)	(−78)	(342)	(−430)	(−88)	(−170)	(−82)
				Midlatitude winter					
232	−317	−85	−147	−62	230	−317	−87	−155	−68
(255)	(−317)	(−92)	(−137)	(−45)	(220)	(−317)	(−97)	(−144)	(−47)
				Subarctic summer					
318	−391	−73	218	−145	314	391	−77	−223	−146
312	(−391)	(−79)	(−209)	(−130)	(−304)	(−391)	(−87)	(−212)	(−125)

cloud base (i.e., the reflectance of the upward irradiance at cloud base) of about 4–6%. Although this reflectance is small, its impact on the flux profiles within the cloud and thus on the cloud heating profiles is substantial. This is because the effects of the small reflectance on the radiative properties of the cloud are exaggerated by the relatively large differences between the flux originating from the warmer atmosphere below the cloud and the cloud fluxes associated with the colder cloud temperatures. Thus the reflectance contribution is most pronounced when such a temperature difference is large which is the case for the tropical atmosphere. Closer analysis of the reflectance revealed that it is directly related to the degree of anisotropy of the scattering.

The effective emittances were presented for $\lambda = 11$ μm and for broad-band calculations. They were found to be sensitive to the single-scattering properties through the dependence of reflectance on the asymmetry parameter of the phase function. The contribution to the effective emittance varied for scattering by cylinders (spheres) from 25% (15%) of the total effective emittance in a tropical atmosphere to 10% (5%) in the McClatchey *et al.* subarctic summer model atmosphere.

The trends portrayed for $\lambda = 11$ μm were evident in the broad-band calculations. It was suggested that the presence of the IR reflectance accounted for the previously reported discrepancies between the broad-band (effective) emittances derived from the observations of Griffith and Cox (1977) and the theoretical estimates. It was also shown that the presence of reflectance significantly modulates the total atmosphere emission particularly in the tropical atmosphere.

The results presented suggest that it is important to parameterize the IR reflectance of high clouds either explicitly together with a formally defined emittance or to include implicitly the reflectance in a parameterized effective emittance form. The parameterization of such single combined parameters will cause problems since the contributions by reflectance to the effective emittance varies according to the state of the atmosphere. The extent of this variation may be realized from the variation of the 11 μm effective emittance shown in Fig. 6 and quoted above.

REFERENCES

Appleman, H. S., 1961: Occurrence of forecasting of cirrostratus clouds. WMO Tech. Note No. 40, No. 109, TP.47, 29 pp.

Feigelson, E. M., 1970: *Radiant Heat Transfer in a Cloudy Atmosphere.* Israel Program for Scientific Translations, 191 pp.

Grant, I. P., and G. E. Hunt, 1968: Solutions of radiative transfer problems in planetary atmospheres. *Icarus,* **9,** 526–534.

Griffith, K. T., and S. K. Cox, 1977: Infrared radiative properties of tropical cirrus inferred from broad band measurements. Atmos. Sci. Pap. No. 269, Colorado State University, 102 pp. [NTIS PB-268531].

Heymsfield, A. J., 1975: Cirrus unicus generating cells and the evolution of cirroform clouds: Part I. Aircraft observations of the growth of the ice phase. *J. Atmos. Sci.,* **32,** 799–808.

Kattawar, G. E., and G. N. Plass, 1967: Electromagnetic scattering from absorbing spheres. *Appl. Opt.,* **6,** 1377–1382.

Kuhn, P. M., and H. K. Weikmann, 1969: High altitude radiometric measurements of cirrus. *J. Appl. Meteor.,* **8,** 147–154.

Liou, K. N., 1972a: Electromagnetic scattering by arbitrarily orientated ice cylinders. *Appl. Opt.,* **11,** 667–674.

——, 1972b: Light scattering by ice clouds in the visible and infrared: A theoretical study. *J. Atmos. Sci.,* **30,** 1303–1326.

——, 1974: On the radiative properties of cirrus in the window region and their influence on remote sensing of the atmosphere. *J. Atmos. Sci.,* **31,** 522–532.

McClatchey, R. A., R. W. Fenn, J. E. Selby, F. E. Volz and J. S. Goring, 1972: Optical properties of the atmosphere, 3rd ed. AFCRL-72-0497, 102 pp.

Platt, C. M. R., 1973: Lidar and radiometric observations of cirrus clouds. *J. Atmos. Sci.,* **30,** 1191–1204.

Rodgers, C. D., and C. D. Walshaw, 1966: The computation of IR cooling rates in planetary atmospheres. *Quart. J. Roy. Meteor. Soc..,* **92,** 67–92.

Roewe, D., and K. N. Liou, 1978: Influence of cirrus clouds on the infrared cooling rate in the troposphere and lower stratosphere. *J. Appl. Meteor.,* **17,** 99–106.

Stephens, G. L., 1976a: The transfer of radiation through vertically nonuniform stratocumulus water clouds. *Contrib. Atmos. Phys.,* **49,** 237–254.

——, 1976b: An improved estimate of IR cooling in the atmospheric window region. *J. Atmos. Sci.,* **32,** 806–809.

——, 1978a: Radiation profiles in extended water clouds. I: Theory. *J. Atmos. Sci.,* **35,** 2111–2122.

——, 1978b: Radiation profiles in extended water clouds. II: Parameterization schemes. *J. Atmos. Sci.,* **35,** 2123–2132.

——, and P. J. Webster, 1979: Sensitivity of radiative forcing to variable cloud and moisture. *J. Atmos. Sci.,* **36,** 1542–1556.

——, and K. J. Wilson, 1980: The sensitivity of a deep cumulus convection model to changes in radiative forcing. *J. Atmos. Sci.* **37,** 421–434.

Van de Hulst, H. C., and K. Grossman, 1968: Multiple light scattering in planetary atmospheres. *The Atmospheres of Venus and Mars,* J. C. Brandt and M. B. McElroy, Eds., Gordon and Breach, 35–45.

Wiscombe, W., 1976: Extension of the doubling method to inhomogeneous sources. *J. Quant. Spectros. Radiat. Transfer,* **16,** 477–489.

——, 1977: The delta M method: Rapid yet accurate radiative flux calculations for strongly asymmetric phase functions. *J. Atmos. Sci.,* **34,** 1408–1422.

——, and J. W. Evans, 1977: Exponential sum fitting of radiative transmission functions. *J. Comput. Phys.,* **24,** 416–444.